

# AIR-HLoc: Adaptive Retrieved Images Selection for Efficient Visual Localisation

Changkun Liu<sup>1</sup>, Jianhao Jiao<sup>2</sup>, Huajian Huang<sup>1</sup>, Zhengyang Ma<sup>3</sup>, Dimitrios Kanoulas<sup>2</sup> and Tristan Braud<sup>1,4</sup>

**Abstract**—State-of-the-art hierarchical localisation pipelines (HLoc) employ image retrieval (IR) to establish 2D-3D correspondences by selecting the top- $k$  most similar images from a reference database. While increasing  $k$  improves localisation robustness, it also linearly increases computational cost and runtime, creating a significant bottleneck. This paper investigates the relationship between global and local descriptors, showing that greater similarity between the global descriptors of query and database images increases the proportion of feature matches. Low similarity queries significantly benefit from increasing  $k$ , while high similarity queries rapidly experience diminishing returns. Building on these observations, we propose an adaptive strategy that adjusts  $k$  based on the similarity between the query’s global descriptor and those in the database, effectively mitigating the feature-matching bottleneck. Our approach optimizes processing time without sacrificing accuracy. Experiments on three indoor and outdoor datasets show that AIR-HLoc reduces feature matching time by up to 30%, while preserving state-of-the-art accuracy. The results demonstrate that AIR-HLoc facilitates a latency-sensitive localisation system.

## I. INTRODUCTION

Visual localisation systems estimate the 6 degrees of freedom (6DoF) absolute camera pose for query images. Accurate and real-time absolute 6DoF pose estimation is crucial in diverse applications, from augmented reality to navigation and decision-making for mobile robots. Standard structure-based methods [1], [2], [3], [4], [5], [6], [7] achieve high accuracy by detecting and matching visual features in query images with a 3D representation of the environment. To reduce the search space in large datasets, standard hierarchical localisation pipelines (HLoc) [3], [7] include an image retrieval (IR) module to establish 2D-2D matches between the query image and the top- $k$  ranked database images. The  $k$  retrieved images are used to produce 2D-3D correspondences based on a smaller subset of the environment 3D model. Camera pose is finally estimated via RANSAC and Perspective-n-Point (PnP) algorithms [8], [9].

These methods typically use a fixed value of  $k$ , determined empirically to balance robustness and performance for a given dataset [10]. The choice of  $k$  is crucial, as it directly impacts localisation accuracy and runtime. This work seeks to optimize  $k$  selection to minimize runtime without

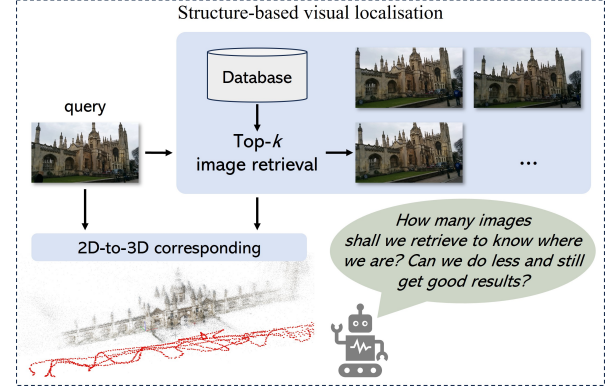


Fig. 1. AIR-HLoc proposes a practical but efficient solution to increase localisation efficiency while maintaining accuracy as a structure-based visual localisation framework.

compromising localisation accuracy. A larger  $k$  increases the number of potential matches from similar images, enhancing localisation robustness for challenging queries and improving overall positioning accuracy. However, it also extends feature matching time, becoming a key bottleneck in the pipeline, and may introduce noisy matches. Conversely, a smaller  $k$  reduces runtime and improves efficiency, but at the cost of localisation accuracy. Previous works [10], [6] recommend using a moderate value of  $k$ , typically between 5 and 30. However, applying a fixed  $k$  for all queries can reduce accuracy (if  $k$  is too small) or waste computational resources and processing time (if  $k$  is too large).

To address this challenge, we explore strategies for achieving a better trade-off by selecting an appropriate  $k$  for each query in real-world latency-sensitive visual localisation systems, as shown in Figure 1. Since global descriptors used in IR methods provide a high-level image representation, we calculate the cosine similarity between the global descriptors of the query image and the top-3 retrievals. This serves as the basis for the scoring mechanism described in Section III-C, which quantifies the query image’s similarity to the reference database images. Our observations indicate that query images with varying scores exhibit different levels of localisation difficulty. Higher scores, representing greater similarity and more local feature matches, correspond to easier localisation, where fewer images are required to establish sufficient 2D-3D correspondences.

Building on this insight, we introduce an adaptive retrieved image selection (AIR) approach for the hierarchical localisation pipeline, AIR-HLoc, which adaptively adjusts the number of retrieved images based on these scores for

<sup>1</sup>Department of Computer Science and Engineering, HKUST, Hong Kong, {cliudg, hhuangbg}@connect.ust.hk. Corresponding author: Tristan Braud, braudt@ust.hk

<sup>2</sup> Department of Computer Science, University College London, London, The United Kingdom, {ucacjji, d.kanoulas}@ucl.ac.uk

<sup>3</sup>Division of Emerging Interdisciplinary Areas, HKUST, Hong Kong, zmaaf@connect.ust.hk

<sup>4</sup>Division of Integrated Systems Design, HKUST, Hong Kong

different queries. This method reduces the number of retrieved images and feature matching cost while maintaining localisation accuracy.

We summarize our main contributions as follows:

- 1) We begin with a statistical analysis of the relationship between global and local descriptors. Across three indoor and outdoor datasets, using three mainstream IR models, we observe that higher image similarity correlates with a greater proportion of feature matches.
- 2) We propose using the cosine similarity of global descriptors to assess the localisation difficulty of queries. Building on this, we introduce an adaptive retrieved images selection (AIR) approach for HLoc. For easier queries, we retrieve fewer images, while for more challenging queries, we retrieve more images. Additionally, we present a novel metric, *retrieve accuracy yield ratio (RAYR)*,  $\zeta$ , to quantify the improvement in localisation accuracy as  $k$  varies across different queries. This insight facilitates more informed  $k$  selection and algorithm design in practical applications.
- 3) Our proposed system, AIR-HLoc, reduces the average matching time by 30%, 26%, and 11% across Cambridge Landmarks, 7Scenes, and Aachen Day-Night-v1.1 datasets, respectively, while maintaining state-of-the-art accuracy. On the Cambridge dataset, AIR-HLoc reduces the average query runtime by 2433 ms at  $k = 10$  on the Jetson Orin platform, while achieving higher accuracy than HLoc.

## II. RELATED WORK

### A. Visual localisation

**Structure-based methods** estimate camera poses by establishing matches between the 2D features of the query image and 3D points of pre-built 3D models. The matches can be established indirectly with local feature extraction and matching [3], [11], [7], [12], [13] or directly with scene coordinate regression [14], [15], [16], [17], [18]. However, even though scene coordinate regression (SCR) methods achieve high accuracy in small and medium indoor scenes, they are not robust and accurate enough for larger and more complex scenes [19], [16], [20]. HLoc pipeline [3], [7], [21] achieves State-of-the-art (SOTA) accuracy on both indoor and large-scale outdoor scenes by using IR [22], [23], [24] as an intermediate step, allowing it to scale up to larger scenes.

**Absolute Pose Regressors** (APRs) are end-to-end learning-based methods that directly regress the absolute camera pose from input images. PoseNet [25], [26] and the follower APRs [27], [28], [29], [30], [31], [32] can provide faster predictions than structure-based methods. However, they have low accuracy and robustness and are very difficult to generalize well to novel viewpoints, which are very different from the training set [33], [34]. Therefore, this paper focuses on the HLoc pipeline, the indirect structure-based approach with IR, because it can provide robust and accurate results in large-scale scenes.

### B. Image Retrieval

Image Retrieval (IR) is commonly used for place recognition and visual localisation tasks. IR fetches top  $k$  relevant and similar database images given query images by extracting global descriptor from pre-trained models [22], [24], [35], [36]. We focus on IR in structure-based localisation in this paper. [10] studies the performance correlation between classical place recognition and localisation tasks and finds almost no improvement in visual localisation when  $k$  is larger than 20. Mobile sensors' data are utilized to reduce the database's research space when doing IR in [37]. [38], [6] use a fusion of global descriptors in the visual localisation task. This study aims to improve the speed of HLoc by adaptively allocating the number of retrieved images for more efficient matching and pose estimation instead of using a constant  $k$  for all queries in previous work.

## III. METHODS

Given a query image  $I^q \in \mathbb{R}^{H \times W \times 3}$ , HLoc predicts a 6DoF camera pose  $\hat{p}_k = [\hat{\mathbf{x}}_k, \hat{\mathbf{q}}_k]$  by retrieving the top- $k$  similar images to  $I^q$ .  $\hat{\mathbf{x}}_k \in \mathbb{R}^3$  denotes the estimated global translation,  $\hat{\mathbf{q}}_k \in \mathbb{R}^4$  denotes the estimated quaternion, which encodes the rotation. In this section, we analyze the impact of the hyperparameter  $k$  on the runtime and localisation accuracy for different query images  $I^q$ . Based on our findings, we propose a novel scheme, AIR-HLoc, to enhance the efficiency of HLoc while maintaining the accuracy.

### A. Problem Formulation

In the HLoc pipeline, given a query image  $I^q$ , an image retrieval (IR) model retrieves the top- $k$  images from a reference database  $D$ , ranked by the cosine similarity of their global descriptors, as illustrated in Figure 1. HLoc then establishes 2D-2D correspondences between the query image  $I^q$  and the retrieved images utilizing feature matching. By combining these 2D-2D correspondences with the 3D scene model, HLoc establishes 2D-3D correspondences between  $I^q$  and the scene, and predicts a 6DoF camera pose  $\hat{p}_k = [\hat{\mathbf{x}}_k, \hat{\mathbf{q}}_k]$ .

Feature matching is the bottleneck of HLoc. The larger the  $k$ , the longer it takes to feature matching. We show the detailed data in Section IV-F. We aim to reduce the feature-matching cost by retrieving top- $k^*$  reference images,  $k^* \leq k$  for different query image  $I^q$  while maintaining robustness and accuracy. We first investigate several mainstream IR methods, AP-GeM [24], NetVLAD [22], and EigenPlaces [35], to show the local descriptors matching is highly corresponding to global visual similarity between query and reference database images and different queries have different benefits for accuracy when increasing the number of  $k$ . So we argue that existing methods retrieve an equal number of images for all queries is a waste of processing time and computation power.

### B. Relationship between match ratio and similarity

Given a query image  $I^q$ , the image database is  $D$ . An IR model  $E$  extracts the global descriptors of the query image  $I^q$

as  $g_q$ .  $E$  extracts the global descriptors of reference images  $I^r, I^r \in D$  as  $g_r$ . The similarity between  $I^q$  and  $I^r$  is

$$\cos(g^q, g^r) = \frac{g^q \cdot g^r}{\|g^q\|_2 \cdot \|g^r\|_2} \quad (1)$$

Similarly, a local feature extraction model  $F$  extracts the local feature of the query image  $I^q$  as  $f_q$ .  $F$  extracts the local feature of  $I^r$  as  $f^r$ . The number of local feature points of  $I^q$  is  $N(f^q)$ , and the number of matched local features between  $f^r$  and  $f^q$  is  $M(f^q, f^r)$ . We define the *match ratio* as:

$$\text{match ratio} = \frac{M(f^q, f^r)}{N(f^q)} \quad (2)$$

, where  $0 \leq \text{match ratio} \leq 1$ . In this paper, we use the prevalent SuperPoint (SP) [12] and SuperGlue (SG) [7] as the feature extractor and matcher.

Figure 2 shows the strong correlation between cosine similarity in Equation 1 and *match ratio*, as described in Equation 2, for each  $I^q$  and  $I^r$  pair. The number in parentheses of each subplot is the Pearson correlation coefficient (PCC) [39] and Spearman correlation coefficient (SRC) [40] ranges from -1 to 1. A larger PCC value indicates a stronger linear positive correlation, while SRC values close to 1 suggest a strong positive monotonic relationship. We opt to use the *match ratio* instead of the absolute number of matches in our analysis, as some query images exhibit textureless regions with fewer feature points, yielding only a few matches even when highly similar images are retrieved. Utilizing a *match ratio* from 0 to 1 provides a more meaningful measure. Our analysis incorporates three distinct IR models (AP-GeM, NetVLAD, and EigenPlaces). AP-GeM and NetVLAD serve as representative IR models in the visual localisation pipeline [6], [3], [10]. A strong positive correlation between *match ratio* and similarity is observed for all three IR models across three different datasets. Therefore, if a query image can find very similar images, then a small number of retrieved images can contribute enough matches for pose estimation. For queries that have difficulty finding similar images, we need more retrieved images.

### C. Adaptive Retrieved Images Selection

According to the correlation observed in Figure 2, we propose to use the similarity between the images in the database and the query to evaluate the localisation difficulty of query images. We first store the global descriptors  $G^r$  of all the images in the reference images database offline. For a query image  $I^q$ , we get the global descriptor  $g^q$  using a pre-train IR model. Then, we calculate the cosine similarity between  $g^q$  and each  $g^r \in G^r$ . The similarity is then ranked from highest to lowest, with the mean of the top  $n$  being the score  $S(I^q)$  of the  $I^q$ .

$$S(I^q) = \frac{1}{n} \sum_{j \in J} \cos(g^q, g^j) \quad (3)$$

where  $J$  represents the indices of the top  $n$  images in the ranked list. In this paper, we set  $n = 3$ . We believe that the three most similar images are sufficient to reflect the

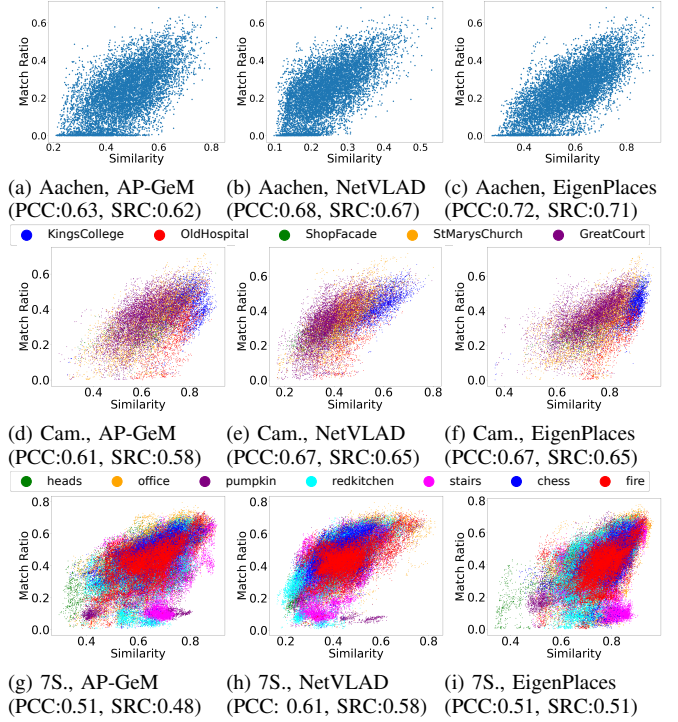


Fig. 2. Subfigures (a)-(f) show the correlation between cosine similarity (-1 to 1) and *match ratio* (0 to 1) in Aachen Day-Night-v1.1 datasets [41], [42], Cambridge landmark [25], and 7Scenes [43], [44] using three IR models (AP-GeM, NetVLAD and EigenPlaces). The value in parentheses of each subfigure is the average PCC and SRC across all scenes in a dataset.

localisation difficulty of this query. Therefore, instead of retrieving fixed  $k$  images for all queries, we retrieve different numbers of reference images for different queries depending on  $S(I^q)$  in Equation (3). We denote the maximum number of images that are retrieved as  $k$  for each  $I^q$ . Then, for different  $I^q$ , we follow the below rules:

- For easy query,  $S(I^q) \geq \gamma^h$ , we retrieve top- $k^*$  images,  $k^* = \lceil \alpha \times k \rceil$ .
- For medium query,  $\gamma^l \leq S(I^q) < \gamma^h$ , we retrieve top- $k^*$  images,  $k^* = \lceil \beta \times k \rceil$ .
- For hard query,  $S(I^q) < \gamma^l$ , we retrieve top- $k$  images.

, where  $\gamma^h$ ,  $0 < \gamma^h \leq 1$  is the high similarity threshold.  $\gamma^l$ ,  $0 < \gamma^l < \gamma^h \leq 1$  is the low similarity threshold.  $0 < \alpha < \beta < 1$  are coefficients to reduce the number of retrieved images.  $\lceil \cdot \rceil$  is the ceiling function. Since we adaptively assign the retrieved number for each  $I^q$ , we call our improved HLoc approach as AIR-HLoc.

### D. Retrieve Accuracy Yield Ratio

To assess the impact of increasing  $k$  on localisation accuracy, we propose a new metric called the *Retrieve Accuracy Yield Ratio* (RAYR), denoted as  $\zeta = (\zeta_T(k), \zeta_R(k))$ . The term  $\zeta_T(k)$  represents the reduction in translation error relative to the baseline  $k = 1$  for a given query image  $I^q$ , while  $\zeta_R(k)$  captures the reduction in rotation error. Higher values of  $\zeta_T(k)$  or  $\zeta_R(k)$  signify a greater average contribution of

the retrieved top- $k$  images to the overall improvement in localisation accuracy.

$$\zeta_T(k) = -\frac{\text{ATE}(k) - \text{ATE}(1)}{k-1}, \quad k \geq 2 \quad (4)$$

$$\zeta_R(k) = -\frac{\text{ARE}(k) - \text{ARE}(1)}{k-1}, \quad k \geq 2 \quad (5)$$

The absolute translation error (ATE) and absolute rotation error (ARE) are defined as follows:  $\text{ATE}(k) = \|\hat{\mathbf{x}}_k - \mathbf{x}\|_2$ ,  $\text{ARE}(k) = 2 \arccos |\mathbf{q}^{-1} \hat{\mathbf{q}}_k| \cdot \frac{180}{\pi}$ . Here,  $\mathbf{q}^{-1}$  denotes the conjugate of the ground truth quaternion  $\mathbf{q}$ , and  $p = [\mathbf{x}, \mathbf{q}]$  represents the ground truth 6DoF camera pose of  $I^q$ .

#### IV. EVALUATION

##### A. Datasets

To fully demonstrate the effectiveness of our approach, we selected three popular visual localisation datasets that encompass indoor scenes, large-scale outdoor scenes, and challenges involving day-night changes, moving objects, and motion blur. The *7Scenes* dataset [43], [44] is an indoor dataset consisting of seven small scenes from  $1m^3$  to  $18m^3$ . We use the rendered depth maps provided by [15] to improve the accuracy of the sparse point cloud. The *Cambridge Landmarks* [25] is a large-scale outdoor dataset with five scenes. The *Aachen Day-Night-v1.1* [41], [42] comprises 6697 training and 1015 test images taken from the Aachen, Germany. The database images were captured during the daytime using handheld cameras, while query images were taken with three mobile phones during both day and night. The test set is divided into two conditions: day and night. Nighttime images are only for testing.

##### B. Implementation details

We integrate NetVLAD and EigenPlaces into AIR-HLoc and conduct visual localisation experiments because these two IR models have stronger correlation with the match ratio than AP-GeM as shown in Figure 2. Different IR methods have an impact on similarity thresholds. As shown in Figure 2, although the correlation between the three IR methods is similar for each dataset, the range distribution of similarity is slightly different. For Eigenplaces, the distribution of similarity on all datasets is 0.3 to 0.95, but NetVLAD and AP-GeM are not so uniform. For NetVLAD in particular, the range of similarity on Aachen Day-Night-v1.1 dataset is smaller than on Cambridge Landmarks and 7Scenes datasets. There should be two reasons for this. Firstly, the Aachen-V1.1 dataset represents a handheld motion pattern for AR applications in city-scale environments, and Eigenplaces is more robust to camera viewpoint changes than NetVLAD and AP-GeM [35]. Secondly, the Aachen Day-Night-v1.1 dataset has the cross-device domain gap that reference images and query images have different resolutions and camera intrinsic parameters, while images of 7scenes and Cambridge datasets were captured with the same camera.

Therefore, for NetVLAD, we set  $\gamma^l = 0.4$  and  $\gamma^h = 0.6$  for Cambridge and 7Scenes datasets,  $\gamma^l = 0.3$  and  $\gamma^h = 0.5$  for

Aachen-V1.1 dataset. For EigenPlaces, We set  $\gamma^l = 0.7$  and  $\gamma^h = 0.9$  for all three datasets. We set  $\alpha = 0.5$  and  $\beta = 0.7$  for all IR methods and all three datasets. We conduct experiment based on the HLoc toolbox [3].

##### C. Evaluation

We evaluate the performance of HLoc and AIR-HLoc through two primary metrics. We consider the mean and median absolute translation error (ATE) and absolute rotation error (ARE) for all test frames in Cambridge Landmarks and 7Scenes datasets. For Aachen Day-Night-v1.1, we analyze the percentage of test images with pose predicted with high ( $0.25m, 2^\circ$ ), medium ( $0.5m, 5^\circ$ ), and low ( $5m, 10^\circ$ ) accuracy levels proposed by [41]<sup>1</sup>.

##### D. Results

We present the localisation accuracy of HLoc and AIR-HLoc across three distinct datasets, as depicted in Figure 3 and Figure 4, with respect to varying values of  $k$ . In the case of HLoc, we report the results for  $k = 1, 2, 3, 4, 5, 10, 20, 30$  and it retrieves the same number of  $k$  images from the database for all queries. For AIR-HLoc, we provide the outcomes for  $k = 4, 5, 10, 20, 30$ , considering a retrieval of top- $k$  similar images solely for hard queries, top- $k^*$ ,  $k^* = \lceil \alpha \times k \rceil$  images for easy queries, and top- $k^*$ ,  $k^* = \lceil \beta \times k \rceil$  images for medium queries. We do not give the results for  $k \leq 3$  because the optimization space is too small and most datasets achieve much higher accuracy when  $k \geq 10$ .

1) *Cambridge Landmarks*: For both HLoc and AIR-HLoc, the mean and median pose errors converge when  $k \geq 10$ . As shown in Figures 3 (a)-(b) and Figure 5 (a), AIR-HLoc achieves nearly the same accuracy as HLoc while retrieving up to 30% fewer images. The performance of both IR modules is comparable. Table I highlights that AIR-HLoc achieves SOTA accuracy compared to other methods.

TABLE I  
COMPARISONS ON CAMBRIDGE LANDMARKS DATASET. WE REPORT THE MEDIAN TRANSLATION AND ROTATION ERRORS (CM/ $^\circ$ ) OF DIFFERENT METHODS. WE REPORT THE RESULTS OF HLOC AND AIR-HLOC USING  $k = 10$ .

	Methods	Kings	Hospital	Shop	Church	Avg. ↓ [cm/ $^\circ$ ]
APR	PoseNet [25]	93/2.73	224/7.88	147/6.62	237/5.94	175/5.79
	MS-Transformer [27]	85/1.45	175/2.43	88/3.20	166/4.12	129/2.80
	LENS [45]	33/0.5	44/0.9	27/1.6	53/1.6	39/1.15
	DFNet [29]	73/2.37	200/2.98	67/2.21	137/4.02	119/2.90
SCR	ACE [17]	29/0.38	31/0.61	5/0.3	19/0.6	21/0.47
	DSAC* [46]	18/0.3	21/0.4	5/0.3	15/0.6	15/0.4
	GLACE [18]	19/0.32	18/0.42	5/0.22	9/0.3	13/0.32
SOTA	PixLoc [47]	14/0.2	16/0.3	5/0.2	10/0.3	11.3/0.25
	HLoc (SP+SG) [7], [12]	11.3/0.2	15/0.31	4.2/0.21	7.1/0.22	9.4/0.24
	<b>AIR-HLoc (SP+SG) (ours)</b>	<b>11.2/0.2</b>	<b>14.6/0.32</b>	<b>4.2/0.20</b>	<b>7.3/0.20</b>	<b>9.3/0.23</b>

2) *7Scenes*: Similarly, for both HLoc and AIR-HLoc, the mean and median pose errors converge when  $k \geq 20$ . Figures 3 (c)-(d) and Figure 5 (a) demonstrate that AIR-HLoc matches HLoc's accuracy while retrieving up to 26%

<sup>1</sup>This dataset does not provide ground truth poses for each test frame.

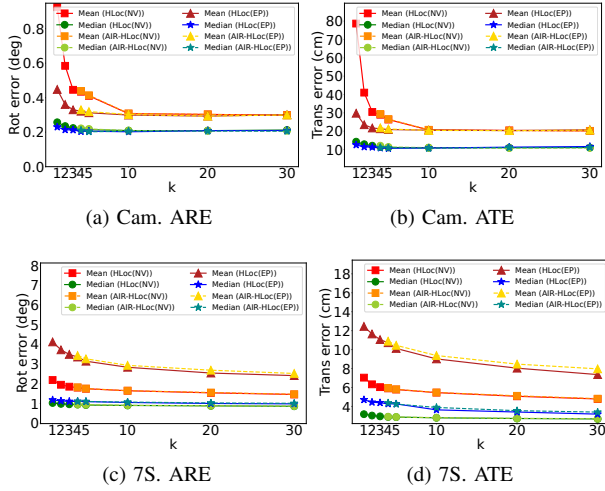


Fig. 3. Average mean and median pose error (ATE, ARE) for Cambridge and 7Scenes datasets across all scenes against  $k$ . For HLoc, it retrieves top- $k$  similar images for all queries. For AIR-HLoc, it retrieves  $k$  similar images only for hard queries and  $k^*$  images for medium and easy queries. AIR-HLoc (NV) uses NetVLAD as the image retrieval module, while AIR-HLoc (EP) utilizes EigenPlaces for image retrieval. The average *retrieved ratio* ( $k^*/k$ ) for all queries is shown in Figure 5 (a).

fewer images. Two IR modules exhibit similar performance. Table II shows that AIR-HLoc and HLoc achieve SOTA accuracy compared to other approaches.

3) *Aachen Day-Night-v1.1*: For both HLoc and AIR-HLoc, the three accuracy levels converge when  $k \geq 20$ . Subfigures 4 (a)-(b) and Figure 5 (a) shows that AIR-HLoc achieves almost the same accuracy of HLoc with up to 11% fewer retrieved images. We find that AIR-HLoc (NetVLAD) has slightly better accuracy than HLoc (NetVLAD) in (0.25m,  $2^\circ$ ) when  $k = 20$ , and AIR-HLoc (EigenPlaces) have slightly better accuracy than HLoc (EigenPlaces) in (0.25m,  $2^\circ$ ) when  $k = 30$  in day-time test sequences. This shows that our AIR-HLoc can improve accuracy by reducing the noisiness introduced by high  $k$  for easy queries.

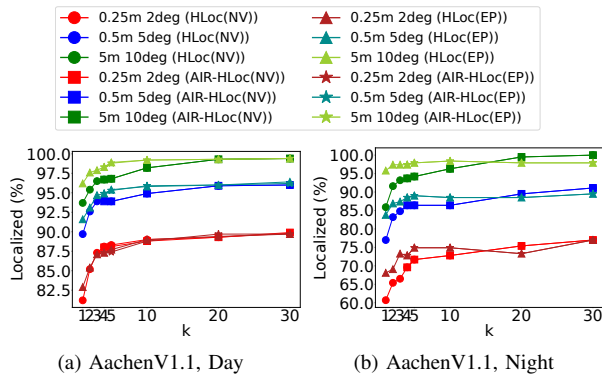


Fig. 4. Percentage (%) of test frames high (0.25m,  $2^\circ$ ), medium (0.5m,  $5^\circ$ ), and low (5m,  $10^\circ$ ) accuracy [41] (higher is better) for HLoc and AIR-HLoc against  $k$ . The average *retrieved ratio* ( $k^*/k$ ) for all queries is shown in Figure 5 (a).

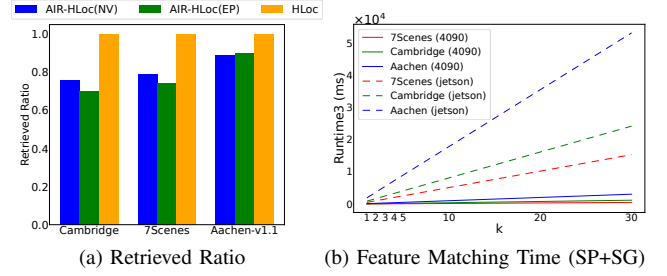


Fig. 5. (a) *Retrieved Ratio* refers to the ratio ( $0 < k^*/k \leq 1$ ) of the average number of retrieved images for AIR-HLoc compared to HLoc for all test frames. (b) The feature matching time (runtime3) of HLoc in SuperPoint (SP) + SuperGlue (SG) setting for three datasets against  $k$ .

## E. Analysis

We present examples of queries classified as easy, medium, and hard alongside their top three retrieved images in Figure 7. Easy query images are very similar to retrieved images, and there are relatively similar images for medium queries. In contrast, for hard queries, the retrieved images are even incorrect, showing no overlap with the query images. As depicted in Figure 6 (a)-(d), increasing  $k$ , primarily improves the accuracy for hard queries. For easy and medium queries, further gains become negligible when  $k \geq 5$ . Furthermore, the average contribution of the top- $k$  images to the overall localisation accuracy converges to zero when  $k \geq 10$  for these query types. As  $k$  increases, the reduction in pose estimation error is primarily observed for hard queries, while easy and medium queries show very limited improvement.

Figures 6 (a)-(b) demonstrate that pose estimation for easy queries is significantly more accurate compared to hard queries, even when  $k$  is sufficiently large. This observation suggests that the similarity score of a query is indicative of the uncertainty in pose estimation. These results highlight the inefficiency of using a fixed number of retrieved images for feature matching across all queries, underscoring the effectiveness of AIR-HLoc.

## F. System Efficiency and Application

We first conduct the runtime analysis using an NVIDIA GeForce GTX 4090 GPU on a desktop. To illustrate the bottleneck introduced by feature matching and its impact on mobile robot localisation tasks, we also evaluate the runtime on an embedded NVIDIA Jetson Orin platform with 64 GB RAM. GTX 4090: We assess the runtime of the entire HLoc pipeline. Since global and local feature extraction for the reference image database can be performed offline, we focus on the runtime for query image feature extraction (runtime1), image retrieval (runtime2), feature matching (runtime3), and pose estimation (runtime4). Runtime1 and runtime4 are nearly constant per query, while runtime2 depends on the size of the image database. For King's College, runtime1 + runtime2 + runtime4 is approximately 40 ms per query. We observe that runtime3 increases linearly with  $k$ , as shown in Figure 5 (b). Runtime3 is longer for Cambridge and Aachen-V1.1 compared to the higher resolution of



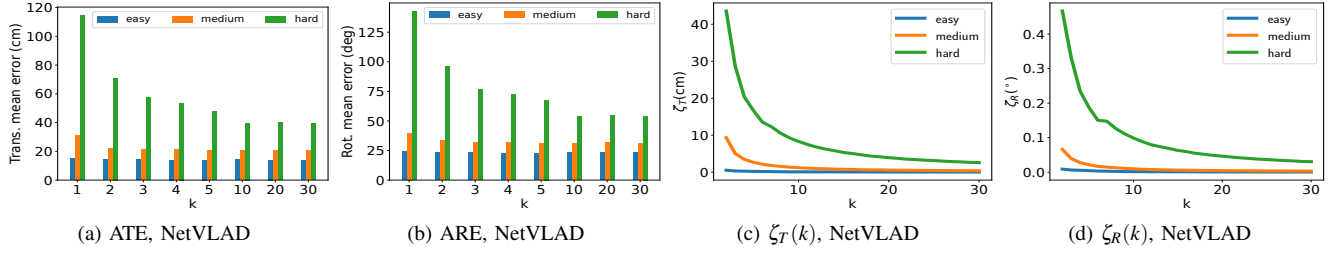


Fig. 6. (a)- (b) Plots of mean rotation and translation errors of HLoc for easy, medium and hard queries of described in Section III-C against  $k$  in Cambridge Landmarks. (c)- (d) The average RAYR,  $\zeta = (\zeta_T(k), \zeta_R(k))$  of all query frames against  $k$  from 1 to 30 in Cambridge Landmarks.

TABLE II

COMPARISONS ON 7SCENES DATASET. THE MEDIAN TRANSLATION AND ROTATION ERRORS (CM/ $^{\circ}$ ) OF DIFFERENT METHODS. THE BEST RESULTS ARE IN BOLD (LOWER IS BETTER). WE REPORT THE RESULTS OF HLOC AND AIR-HLOC USING  $k = 30$ .

	Methods	Chess	Fire	Heads	Office	Pumpkin	Redkitchen	Stairs	Avg. ↓ [cm/ $^{\circ}$ ]
APR	PoseNet [25]	32/8.12	47/14.4	29/12.0	48/7.68	47/8.42	59/8.64	47/13.8	44/10.4
	MS-Transformer [27]	11/4.66	24/9.60	14/12.2	17/5.66	18/4.44	17/5.94	17/5.94	18/7.28
	DFNet [29]	5/1.88	17/6.45	6/3.63	8/2.48	10/2.78	22/5.45	16/3.29	12/3.71
	Marepo [32]	2.6/1.35	2.5/1.42	2.3/2.21	3.6/1.44	4.2/1.55	5.1/1.99	6.7/1.83	3.9/1.68
SCR	DSAC* [46]	<b>1.9/1.1</b>	<b>1.9/1.2</b>	1.1/1.8	<b>2.6/1.2</b>	4.2/1.4	<b>3.0/1.7</b>	4.2/1.4	<b>2.7/1.4</b>
	ACE [17]	<b>1.9/0.7</b>	<b>1.9/0.9</b>	<b>0.9/0.6</b>	<b>2.7/0.8</b>	4.2/1.1	4.2/1.3	<b>3.9/1.1</b>	2.8/0.93
SOTA	HLoc (SP+SG)	2.1/ <b>0.7</b>	<b>1.9/0.8</b>	1.1/0.7	<b>2.6/0.8</b>	<b>3.9/1.0</b>	3.2/ <b>1.1</b>	<b>3.9/1.0</b>	<b>2.7/0.87</b>
	<b>AIR-HLoc (SP+SG)(ours)</b>	2.2/ <b>0.7</b>	<b>1.9/0.8</b>	1.1/0.7	<b>2.6/0.8</b>	<b>3.9/1.0</b>	3.2/ <b>1.1</b>	<b>3.9/1.0</b>	<b>2.7/0.87</b>



Fig. 7. Examples of easy, hard, queries and corresponding top-3 retrieved images in Cambridge Landmarks. Left side are query images in the test set, right side are reference images retrieved by the EigenPlaces model.

images in these datasets<sup>2</sup>. The average runtime<sup>3</sup> per image pair is 17 ms for 7Scenes, 40 ms for Cambridge, and 107 ms for Aachen-V1.1. Runtime<sup>3</sup> dominates the pipeline's execution time when  $k \geq 10$ , while most datasets require at least  $k = 10$  for optimal performance. At  $k = 10$ , AIR-HLoc reduces the average runtime<sup>3</sup> across all queries by 44 ms, 120 ms, and 110 ms for 7Scenes, Cambridge, and Aachen-V1.1, respectively. Jetson Orin: The average runtime<sup>3</sup> per image pair is 510 ms for 7Scenes, 811 ms for Cambridge, and 1900 ms for Aachen-V1.1. At  $k = 10$ , AIR-HLoc reduces the average runtime<sup>3</sup> across all queries by 1326 ms, 2433 ms, and 2090 ms for 7Scenes, Cambridge, and Aachen-

<sup>2</sup>We resize Aachen Day-Night-v1.1 images to a maximum size of 1600 pixels and Cambridge landmarks images to 1024 pixels. For 7Scenes, we retain the original resolution of 640x480 pixels.

V1.1, respectively. It shows that our AIR-HLoc significantly reduces the computational time on a mobile robot platform.

Modern robots often utilize visual-inertial odometry (VIO) to maintain local camera pose tracking [48], [49], [50]. Absolute pose estimation is primarily needed for initial alignment and periodic recalibration of the tracking system. Given that VIO systems are increasingly resilient to drift, they can skip isolated difficult queries, relying instead on easier ones with higher accuracy and lower runtime. This approach, combined with AIR-HLoc, further reduces the computational load for real-time camera relocalisation while maintaining tracking accuracy.

## V. CONCLUSIONS

The IR module in HLoc identifies the top- $k$  similar images from a database of reference images for a query image. Increasing  $k$  enhances localisation robustness for challenging queries but also leads to increased computational cost for feature matching. Feature matching is the bottleneck of the runtime, increasing linearly with  $k$ . This paper introduces AIR-HLoc, a method that optimizes processing time by adaptively retrieve different number of images based on the similarity between query images and the reference image database. Extensive experiments conducted on three datasets demonstrate the efficacy of our algorithm, achieving a reduction by up to 30% in matching cost while maintaining SOTA accuracy. This paper provides novel insights into the relationship between global and local descriptors, offering a deeper understanding that can inform more effective  $k$  selection and algorithm design for practical applications.

## REFERENCES

- [1] T. Sattler, T. Weyand, B. Leibe, and L. Kobbelt, "Image retrieval for image-based localization revisited," in *BMVC*, vol. 1, no. 2, 2012, p. 4.
- [2] M. Dusmanu, I. Rocco, T. Pajdla, M. Pollefeys, J. Sivic, A. Torii, and T. Sattler, "D2-net: A trainable cnn for joint description and detection of local features," in *Proceedings of the IEEE/CVF conference on computer vision and pattern recognition*, 2019, pp. 8092–8101.
- [3] P.-E. Sarlin, C. Cadena, R. Siegwart, and M. Dymczyk, "From coarse to fine: Robust hierarchical localization at large scale," in *Proceedings of the IEEE/CVF Conference on Computer Vision and Pattern Recognition*, 2019, pp. 12716–12725.
- [4] H. Taira, M. Okutomi, T. Sattler, M. Cimpoi, M. Pollefeys, J. Sivic, T. Pajdla, and A. Torii, "Inloc: Indoor visual localization with dense matching and view synthesis," in *Proceedings of the IEEE Conference on Computer Vision and Pattern Recognition*, 2018, pp. 7199–7209.
- [5] H. Germain, G. Bourmaud, and V. Lepetit, "Sparse-to-dense hypercolumn matching for long-term visual localization," in *2019 International Conference on 3D Vision (3DV)*. IEEE, 2019, pp. 513–523.
- [6] P.-E. Sarlin, M. Dusmanu, J. L. Schönberger, P. Speciale, L. Gruber, V. Larsson, O. Miksik, and M. Pollefeys, "Lamar: Benchmarking localization and mapping for augmented reality," in *European Conference on Computer Vision*. Springer, 2022, pp. 686–704.
- [7] P.-E. Sarlin, D. DeTone, T. Malisiewicz, and A. Rabinovich, "Superglue: Learning feature matching with graph neural networks," in *Proceedings of the IEEE/CVF conference on computer vision and pattern recognition*, 2020, pp. 4938–4947.
- [8] L. Kneip, D. Scaramuzza, and R. Siegwart, "A novel parametrization of the perspective-three-point problem for a direct computation of absolute camera position and orientation," in *CVPR 2011*. IEEE, 2011, pp. 2969–2976.
- [9] M. A. Fischler and R. C. Bolles, "Random sample consensus: a paradigm for model fitting with applications to image analysis and automated cartography," *Communications of the ACM*, vol. 24, no. 6, pp. 381–395, 1981.
- [10] M. Humenberger, Y. Cabon, N. Pion, P. Weinzaepfel, D. Lee, N. Guérin, T. Sattler, and G. Csorika, "Investigating the role of image retrieval for visual localization: An exhaustive benchmark," *International Journal of Computer Vision*, vol. 130, no. 7, pp. 1811–1836, 2022.
- [11] D. G. Lowe, "Distinctive image features from scale-invariant keypoints," *International journal of computer vision*, vol. 60, pp. 91–110, 2004.
- [12] D. DeTone, T. Malisiewicz, and A. Rabinovich, "Superpoint: Self-supervised interest point detection and description," in *Proceedings of the IEEE conference on computer vision and pattern recognition workshops*, 2018, pp. 224–236.
- [13] M. Tyszkiewicz, P. Fua, and E. Trulls, "Disk: Learning local features with policy gradient," *Advances in Neural Information Processing Systems*, vol. 33, pp. 14 254–14 265, 2020.
- [14] E. Brachmann, A. Krull, S. Nowozin, J. Shotton, F. Michel, S. Gumhold, and C. Rother, "DSAC-Differentiable RANSAC for camera localization," in *CVPR*, 2017.
- [15] E. Brachmann and C. Rother, "Visual camera re-localization from RGB and RGB-D images using DSAC," *TPAMI*, 2021.
- [16] —, "Learning less is more - 6D camera localization via 3D surface regression," in *CVPR*, 2018.
- [17] E. Brachmann, T. Cavallari, and V. A. Prisacariu, "Accelerated coordinate encoding: Learning to relocalize in minutes using rgb and poses," in *Proceedings of the IEEE/CVF Conference on Computer Vision and Pattern Recognition*, 2023, pp. 5044–5053.
- [18] F. Wang, X. Jiang, S. Galliani, C. Vogel, and M. Pollefeys, "Glance: Global local accelerated coordinate encoding," in *Proceedings of the IEEE/CVF Conference on Computer Vision and Pattern Recognition*, 2024, pp. 21 562–21 571.
- [19] E. Brachmann and C. Rother, "Expert sample consensus applied to camera re-localization," in *Proceedings of the IEEE/CVF International Conference on Computer Vision*, 2019, pp. 7525–7534.
- [20] X. Li, S. Wang, Y. Zhao, J. Verbeek, and J. Kannala, "Hierarchical scene coordinate classification and regression for visual localization," in *Proceedings of the IEEE/CVF Conference on Computer Vision and Pattern Recognition*, 2020, pp. 11 983–11 992.
- [21] J. He, H. Huang, S. Zhang, J. Jiao, C. Liu, and M. Liu, "Accurate prior-centric monocular positioning with offline lidar fusion," in *2024 IEEE International Conference on Robotics and Automation (ICRA)*. IEEE, 2024, pp. 11 934–11 940.
- [22] R. Arandjelovic, P. Gronat, A. Torii, T. Pajdla, and J. Sivic, "Netvlad: Cnn architecture for weakly supervised place recognition," in *Proceedings of the IEEE conference on computer vision and pattern recognition*, 2016, pp. 5297–5307.
- [23] Y. Ge, H. Wang, F. Zhu, R. Zhao, and H. Li, "Self-supervising fine-grained region similarities for large-scale image localization," in *European Conference on Computer Vision*, 2020.
- [24] A. Gordo, J. Almazan, J. Revaud, and D. Larlus, "End-to-end learning of deep visual representations for image retrieval," *IJCV*, 2017.
- [25] A. Kendall, M. Grimes, and R. Cipolla, "Posenet: A convolutional network for real-time 6-dof camera relocalization," in *Proceedings of the IEEE international conference on computer vision*, 2015, pp. 2938–2946.
- [26] A. Kendall and R. Cipolla, "Geometric loss functions for camera pose regression with deep learning," in *IEEE conference on computer vision and pattern recognition*, 2017, pp. 5974–5983.
- [27] Y. Shavit, R. Ferens, and Y. Keller, "Learning multi-scene absolute pose regression with transformers," in *IEEE/CVF International Conference on Computer Vision*, 2021, pp. 2733–2742.
- [28] S. Chen, Z. Wang, and V. Prisacariu, "Direct-posenet: absolute pose regression with photometric consistency," in *2021 International Conference on 3D Vision (3DV)*. IEEE, 2021, pp. 1175–1185.
- [29] S. Chen, X. Li, Z. Wang, and V. A. Prisacariu, "Dfnet: Enhance absolute pose regression with direct feature matching," in *ECCV 2022. Tel Aviv, Israel, October 23–27, 2022, Part X*. Springer, 2022.
- [30] S. Brahmabhatt, J. Gu, K. Kim, J. Hays, and J. Kautz, "Geometry-aware learning of maps for camera localization," in *IEEE conference on computer vision and pattern recognition*, 2018.
- [31] A. Moreau, N. Piasco, D. Tsishkou, B. Stanculescu, and A. de La Fortelle, "Coordinet: uncertainty-aware pose regressor for reliable vehicle localization," in *IEEE/CVF Winter Conference on Applications of Computer Vision*, 2022.
- [32] S. Chen, T. Cavallari, V. A. Prisacariu, and E. Brachmann, "Map-relative pose regression for visual re-localization," in *Proceedings of the IEEE/CVF Conference on Computer Vision and Pattern Recognition*, 2024, pp. 20 665–20 674.
- [33] T. Sattler, Q. Zhou, M. Pollefeys, and L. Leal-Taixe, "Understanding the limitations of cnn-based absolute camera pose regression," in *IEEE/CVF conference on computer vision and pattern recognition*, 2019.
- [34] C. Liu, S. Chen, Y. Zhao, H. Huang, V. Prisacariu, and T. Braud, "Hr-apr: Apr-agnostic framework with uncertainty estimation and hierarchical refinement for camera relocalisation," in *2024 IEEE International Conference on Robotics and Automation (ICRA)*, 2024, pp. 8544–8550.
- [35] G. Berton, G. Trivigno, B. Caputo, and C. Masone, "Eigenplaces: Training viewpoint robust models for visual place recognition," in *Proceedings of the IEEE/CVF International Conference on Computer Vision (ICCV)*, October 2023, pp. 11 080–11 090.
- [36] P. Yin, J. Jiao, S. Zhao, L. Xu, G. Huang, H. Choset, S. Scherer, and J. Han, "General place recognition survey: Towards real-world autonomy," *arXiv preprint arXiv:2405.04812*, 2024.
- [37] S. Yan, Y. Liu, L. Wang, Z. Shen, Z. Peng, H. Liu, M. Zhang, G. Zhang, and X. Zhou, "Long-term visual localization with mobile sensors," in *Proceedings of the IEEE/CVF Conference on Computer Vision and Pattern Recognition*, 2023, pp. 17 245–17 255.
- [38] M. Humenberger, Y. Cabon, N. Guérin, J. Morat, J. Revaud, P. Rerole, N. Pion, C. de Souza, V. Leroy, and G. Csorika, "Robust image retrieval-based visual localization using kapture. arxiv 2020," *arXiv preprint arXiv:2007.13867*, 2007.
- [39] K. Pearson, "VII. note on regression and inheritance in the case of two parents," *proceedings of the royal society of London*, vol. 58, no. 347–352, pp. 240–242, 1895.
- [40] J. L. Myers, A. D. Well, and R. F. Lorch Jr, *Research design and statistical analysis*. Routledge, 2013.
- [41] T. Sattler, W. Maddern, C. Toft, A. Torii, L. Hammarstrand, E. Stenborg, D. Safari, M. Okutomi, M. Pollefeys, J. Sivic, *et al.*, "Benchmarking 6dof outdoor visual localization in changing conditions," in *Proceedings of the IEEE conference on computer vision and pattern recognition*, 2018, pp. 8601–8610.
- [42] Z. Zhang, T. Sattler, and D. Scaramuzza, "Reference pose generation for long-term visual localization via learned features and view synthesis," *International Journal of Computer Vision*, vol. 129, pp. 821–844, 2021.

- [43] B. Glocker, S. Izadi, J. Shotton, and A. Criminisi, "Real-time rgb-d camera relocalization," in *2013 IEEE International Symposium on Mixed and Augmented Reality (ISMAR)*. IEEE, 2013, pp. 173–179.
- [44] J. Shotton, B. Glocker, C. Zach, S. Izadi, A. Criminisi, and A. Fitzgibbon, "Scene coordinate regression forests for camera relocalization in rgb-d images," in *Proceedings of the IEEE conference on computer vision and pattern recognition*, 2013, pp. 2930–2937.
- [45] A. Moreau, N. Piasco, D. Tsishkou, B. Stanciulescu, and A. de La Fortelle, "Lens: Localization enhanced by nerf synthesis," in *Conference on Robot Learning*. PMLR, 2022, pp. 1347–1356.
- [46] E. Brachmann and C. Rother, "Visual camera re-localization from rgb and rgb-d images using dsac," *IEEE transactions on pattern analysis and machine intelligence*, vol. 44, no. 9, pp. 5847–5865, 2021.
- [47] P.-E. Sarlin, A. Unagar, M. Larsson, H. Germain, C. Toft, V. Larsson, M. Pollefeys, V. Lepetit, L. Hammarstrand, F. Kahl, *et al.*, "Back to the future: Learning robust camera localization from pixels to pose," in *Proceedings of the IEEE/CVF conference on computer vision and pattern recognition*, 2021, pp. 3247–3257.
- [48] H. Yu, Y. Feng, W. Ye, M. Jiang, H. Bao, and G. Zhang, "Improving feature-based visual localization by geometry-aided matching," *arXiv preprint arXiv:2211.08712*, 2022.
- [49] H. Bao, W. Xie, Q. Qian, D. Chen, S. Zhai, N. Wang, and G. Zhang, "Robust tightly-coupled visual-inertial odometry with pre-built maps in high latency situations," *IEEE Transactions on Visualization and Computer Graphics*, vol. 28, no. 5, pp. 2212–2222, 2022.
- [50] C. Liu, Y. Zhao, and T. Braud, "Mobilearloc: On-device robust absolute localisation for pervasive markerless mobile ar," in *2024 IEEE International Conference on Pervasive Computing and Communications Workshops and other Affiliated Events (PerCom Workshops)*. IEEE, 2024, pp. 544–549.